A Hybrid Ensemble Learning Approach to Star-galaxy Classification

Edward J. Kim[*][1], Robert J. Brunner[2], and Matias Carrasco Kind[3]

[1] *Department of Physics, University of Illinois, Urbana, IL 61801 USA*
[2] *Department of Astronomy, University of Illinois, Urbana, IL 61801 USA*
[3] *National Center for Supercomputing Applications, Urbana, IL 61801 USA*

13 April 2015

ABSTRACT
Abstract goes here.

Key words: keywords

1 INTRODUCTION

The problem of star-galaxy classification is fundamental to astronomy and goes as far back as **?**. A variety of different strategies have been developed to tackle this long-standing problem, and yet it remains an unsolved challenge. The most commonly used method to classify stars and galaxies in large sky surveys is the morphological separation (**??????**). It relies on the assumption that stars appear as point sources while galaxies appear as resolved sources. However, currently ongoing and upcoming large photometric surveys, such as the Dark Energy Survey (DES[1]) and the Large Synoptic Survey Telescope (LSST[2]), will detect a vast number of unresolved galaxies at faint magnitudes. Near a survey's limit, the photometric observations cannot reliably separate stars from unresolved galaxies by morphology alone without leading to incompleteness and contamination in the star and galaxy samples.

The contamination of unresolved galaxies can be mitigated by using training based algorithms. Machine learning methods have the advantage that it is easier to include extra information, such as concentration indices, shape information, or different model magnitudes. However, they are only reliable within the limits of the training data, and it can be difficult to extrapolate these algorithms outside the parameter range of the training data. These techniques can be further categorized into supervised and unsupervised learning approaches.

In supervised learning, the input attributes (e.g., magnitudes or colors) are provided along with the truth labels (e.g., star or galaxy). **?** pioneered the application of neural networks to the star-galaxy classification problem, and it has become a core part of the astronomical image processing software SExtractor (**?**). Other successfully implemented examples include decision trees (**???**) and Support Vector Machines (**?**). Unsupervised machine learning techniques are less common as they do not utilize the truth labels during the training process and only the input attributes are used.

Physically based template fitting methods have also been used for the star-galaxy classification problem (**??**). Template fitting approaches infer a source's properties by finding the best match between the measured set of magnitudes (or colors) and the synthetic set of magnitudes (or colors) computed from a set of spectral templates. Although it is not necessary to obtain a high-quality spectroscopic training sample, these techniques do require a representative sample of theoretical or empirical templates that span the possible spectral energy distributions (SEDs) of stars and galaxies. Furthermore, they are not exempt from uncertainties due to measurement errors on the filter response curves, or from mismatches between the observed magnitudes and the template SEDs.

In this paper, we present a novel star-galaxy classification framework that combines and fully exploits different classification techniques to produce a more robust classification. In particular, we show that the combination of a morphological separation method, a template fitting technique, a supervised machine learning method, and an unsupervised machine learning algorithm can improve the overall performance over any individual method. In Section 2, we describe each of the star-galaxy classification methods. In Section 3, we describe different classification combination techniques In Section 4, we describe the Canada-France Hawaii Telescope Lensing Survey (CFHTLenS) data set with which we test the algorithms. In Section 5, we compare the performance of our combination techniques to the performance of the individual classification techniques.

2 CLASSIFICATION METHODS

In this section, we present four distinct star-galaxy classification techniques. The first method is a supervised machine learning technique named TPC (Trees for Probabilistic Classification), which uses prediction trees and a random forest (**?**). The second method is an unsupervised machine learning technique named SOMc, which uses self-organizing maps (SOM) and a random atlas to provide a classification citepcarrascokind2014somz. The third method is a Hierarchical Bayesian
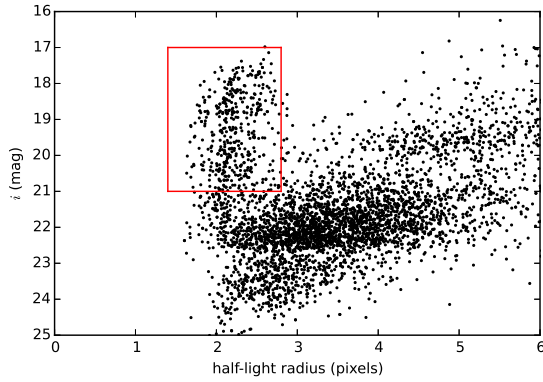
[*] jkim575@illinois.edu
[1] http://www.darkenergysurvey.org/
[2] http://www.lsst.org/lsst/

Figure 1. Half-light radius (r_h) vs. magnitude.

template fitting technique based on the work by **?**, which fits SED templates from star and galaxy libraries to an observed set of measured flux values. The fourth method is a morphological separation method, which uses a hard cut in the half-light radius vs. magnitude plane.

Collectively, these four methods represent the majority of all standard star-galaxy classification approaches published in the literature. It is very likely that any new classification technique would be functionally similar to one of these four methods. Therefore, any of these four methods could in principle be replaced by a similar method.

2.1 Morphological Separation

The simplest and perhaps the most widely used approach to star-galaxy classification is to make a hard cut in the space of photometric attributes. As a first-order morphological selection of point sources, we adopt a technique that is popular among the weak lensing community (**?**). As Figure 1 shows, there is a distinct locus produced by point sources in the half-light radius (r_h; estimated by SExtractor's **FLUX_RADIUS** parameter) vs. the i-band magnitude plane. A rectangular cut in this size-magnitude plane separates point sources, which are presumed to be stars, from resolved sources, which are presumed to be galaxies. The boundaries of the selection box are determined by manually inspecting the size-magnitude diagram.

One of the disadvantages of such cut-based methods is that it classifies every source with absolute certainty. It is difficult to justify such a decisive classification near a survey's magnitude limits, where measurement uncertainties generally increase. A more informative approach is to provide probabilistic classifications. Although a recent work by **?** implemented a probabilistic classification using a Bayesian approach on the morphological measurements alone, here we use a cut-based morphological separation to demonstrate the advantages of our combination techniques. In particular, we later show that the binary output (i.e., 0 or 1) of cut-based methods can be transformed into a probability estimate by combining them with the probability outputs from other probabilistic classification techniques, such as `TPC`, `SOMc`, and `HB`.

2.2 Supervised Machine Learning: TPC

`TPC` is a parallel, supervised machine learning algorithm that uses prediction trees and random forest techniques (**??**) to produce star-galaxy classification. `TPC` is a part of a publicly available software package called `MLZ`[3] (Machine Learning for Photo-z). The full software package includes, among other capabilities, `TPZ`, a supervised photo-z technique (regression mode; **?**), `TPC`, a supervised star-galaxy classification technique (classification mode), `SOM`z, an unsupervised photo-z technique (regression mode; **?**), and `SOMc`, an unsupervised star-galaxy classification technique (classification mode).

`TPC` uses classification trees, a type of prediction trees that are designed to provide a classification or predict a discrete category. Prediction trees are built by asking a sequence of questions that recursively split the data into branches until a terminal leaf is created that meets a stopping criterion (e.g., a minimum leaf size). The optimal split dimension is decided by choosing the attribute that maximizes the *Information Gain* (I_G), which is defined as

$$I_G\left(D_{\mathrm{node}}, X\right) = I_d\left(D_{\mathrm{node}}\right) - \sum_{x \in \mathrm{values}(X)} \frac{|D_{\mathrm{node},x}|}{|D_{\mathrm{node}}|} I_d\left(D_{\mathrm{node},x}\right), \tag{1}$$

where D_{node} is the training data in a given node, X is one of the possible dimensions (e.g., magnitudes or colors) along which the node is split, and x are the possible values of a specific dimension X. $|D_{\mathrm{node}}|$ and $|D_{\mathrm{node},x}|$ are the size of the total training data and the number of objects in a given subset x within the current node, respectively. I_d is the impurity degree index, and `TPC` can calculate I_d from any of the three standard different impurity indices: *information entropy*, *Gini impurity*, and *classification error*. Here, we use the information entropy, which is defined similarly to the thermodynamic entropy:

$$I_d\left(D\right) = -f_g \log_2 f_g - \left(1 - f_g\right) \log_2 f_g, \tag{2}$$

where f_g is the fraction of galaxies in the training data. At each node in our tree, we scan all dimensions to identify the split point that maximizes the information gain as defined by Equation 1, and select the attribute that maximizes the impurity index overall.

In a technique called random forest, we create bootstrap samples (i.e., N randomly selected objects with replacement) from the input training data by sampling repeatedly from the magnitudes using the magnitude errors. We use these bootstrap samples to construct multiple, uncorrelated prediction trees whose individual predictions are aggregated to produce a star-galaxy classification for each source.

We also use a cross validation technique called Out-of-Bag (OOB; **??**). When a tree (or a map) is built in `TPC` (or `SOMc`), a fraction of the training data, usually one-third, is left out and not used in training the trees or maps. After a tree is constructed using two-thirds of the training data, the final tree is applied to the remaining one-third to make a classification. This process is repeated for every tree, and the predictions from each tree are aggregated for each object to make the final star-galaxy classification. We emphasize that if an object is used for training a given tree, it is never used for subsequent prediction by that tree. Thus, the OOB data is an unbiased estimation of the errors and can be used as cross-validation data as long as the OOB data remain similar to the final test data set. The OOB technique can also provide extra information

---

[3] http://lcdm.astro.illinois.edu/code/mlz.html

such as a ranking of the relative importance of the input attributes used in the prediction. The OOB technique can prove extremely valuable when calibrating the algorithm, when deciding which attributes to incorporate in the construction of the trees, and when combining this approach with other techniques.

2.3 Unsupervised Machine Learning: SOMc

A Self-Organizing Map (SOM; **??**) is an unsupervised, artificial neural network algorithm that is capable of projecting high-dimensional input data onto a low-dimensional map through a process of competitive learning. In astronomical applications, the high-dimensional input data can be magnitudes, colors, or some other photometric attributes. The output map is usually chosen to be two-dimensional for the visualization. The differences between a SOM and other neural network algorithms are that a SOM is unsupervised, there are no hidden layers and therefore no extra parameters, and it produces a direct mapping between the training set and the output network. In fact, a SOM can be viewed as a non-linear generalization of a principal component analysis (PCA) algorithm.

The key characteristic of SOM is that it retains the topology of the input training set, revealing correlations between input data that are not obvious. The method is unsupervised: the user is not required to specify the desired output during the creation of the lower-dimensional map, and the mapping of the components from the input vectors is a natural outcome of the competitive learning process.

During the construction of a SOM, each node on the two-dimensional map is represented by weight vectors of the same dimension as the number of attributes used to create the map itself. In an iterative process, each object in the input sample is individually used to correct these weight vectors. This correction is determined so that the specific neuron (or node), which at a given moment best represents the input source, is modified along with the weight vectors of that node's neighboring neurons. As a result, this sector within the map becomes a better representation of the current input object. This process is repeated for every object in the training data, and the entire process is repeated for several iterations. Eventually, the SOM converges to its final form where the training data is separated into groups of similar features.

In a similar approach to random forest in `TPZ` and `TPC`, `SOM`z uses a technique called *random atlas* to provide photo-z estimation (**?**). In random atlas, the prediction trees of random forest are replaced by maps, and each map is constructed from different bootstrap samples of the training data. Furthermore, we create random realizations of the training data by perturbing the input attributes by their measurement error. For each map, we can either use all available attributes, or randomly select a subsample of the attribute space. This SOM implementation can also be applied to the classification problem, and we refer to it as `SOMc` in order to differentiate it from the photo-z estimation problem (regression mode). We also use the random atlas approach in some of the classification combination approaches as discussed in Section 3.

One of the most important parameter in `SOMc` is the topology of the two-dimensional SOM, which can be rectangular, hexagonal, or spherical. To classify stars and galaxies in the CFHTLenS data, we use a spherical topology, which is constructed by using `HEALPIX` (**?**). Furthermore, similar to `TPC`, we

use the OOB technique to make an unbiased estimation of errors. For a complete description of the SOM implementation and its application to the estimation of photo-z probability distribution functions, we refer the reader to **?**.

2.4 Template fitting: Hierarchical Bayesian

One of the most common methods to classify a source based on its observed magnitudes is template fitting. Template fitting algorithms do not require a spectroscopic training sample; there is no need for additional knowledge outside the observed data and the template SEDs. However, any incompleteness in our knowledge of the template SEDs that fully span the possible SEDs of observed sources may lead to misclassification of sources.

Bayesian algorithms use Bayesian inference to quantify the relative probability that each template matches the input photometry and determines a probability estimate by computing the posterior that a source is a star or a galaxy. In this work, we have modified and parallelized a publicly available Hierarchical Bayesian (HB) template fitting algorithm by **?**. In this section, we provide a brief description of the HB template fitting technique; for the details of the underlying HB approach, we refer the reader to **?**.

We write the posterior probability that a source is a star as

$$P\left(S|\mathbf{x}, \theta\right) = P\left(\mathbf{x}|S, \theta\right) P\left(S|\theta\right), \qquad (3)$$

where $\mathbf{x}$ represents a given set of observed magnitudes,. We have also introduced the *hyperparameter* θ, a nuisance parameter that characterizes our uncertainty in the prior distribution. To compute the likelihood that a source is a star, we marginalize over all star and galaxy templates $\mathbf{T}$. In a template-fitting approach, we marginalize by summing up the likelihood that a source has the set of magnitudes $\mathbf{x}$ for a given star template as well as the likelihood for a given galaxy template:

$$P\left(\mathbf{x}|S, \theta\right) = \sum_{t \in \mathbf{T}} P\left(\mathbf{x}|S, t, \theta\right) P\left(t|S, \theta\right). \qquad (4)$$

The likelihood of each template $P\left(\mathbf{x}|S, \theta\right)$ is itself marginalized over the uncertainty in the template-fitting coefficient. Furthermore, for galaxy templates, we introduce another step that marginalizes the likelihood by redshifting a given galaxy template by a factor of $1 + z$.

Marginalization in Equation 4 requires that we specify the prior probability $P\left(t|S, \theta\right)$ that a source has spectral template t (at a given redshift). Thus, the probability that a source is a star (or a galaxy) is either the posterior probability itself if a prior is used, or the likelihood itself if an uniformative prior is used. In a Bayesian analysis, it is preferable to use a prior, which can be directly computed either from physical assumptions, from an empirical function calibrated by using a spectroscopic training sample, or from an empirical function calibrated by using machine learning techniques. In an HB approach, the entire sample of sources is used to infer the prior probabilities for each individual source.

Since the templates are discrete in both SED shape and physical properties, we parametrize the prior probability of each template as a discrete set of weights such that

$$\sum_{t \in \mathbf{T}} P\left(t|S, \theta\right) = 1. \tag{5}$$

These weights correspond to the hyperparameters, which can be inferred by sampling the posterior probability distribution in the hyperparameter space. For the sampling, we use `emcee`, a Python implementation of the affine-invariant Markov Chain Monte Carlo (MCMC) ensemble sampler (**?**).

As the goal of template fitting methods is to minimize the difference between observed and theoretical magnitudes, this approach heavily relies on both the use of SED templates and the accuracy of the transmission functions for the filters used for particular survey. For our stellar templates, we use the empirical SED library from **?**. The Pickles library consists of 131 stellar templates, which span all normal spectral types and luminosity classes at solar abundance, as well as metal-poor and metal-rich F-K dwarf and G-K giant and supergiant stars. We supplement the stellar library with 100 SEDs from **?**, which include low mass stars and brown dwarfs with different T_{eff} and surface gravities. We also include four white dwarf templates of **?**. For our galaxy templates, we use the four CWW spectra from **?**, which include an Elliptical, an Sba, an Sbb, and an Irregular galaxy template. When extending an analysis to higher redshift, the CWW library is often augmented with two star bursting galaxy templates from **?**. From the six original CWW and Kinney spectra, intermediate templates are created by interpolation for a total of 51 SEDs.

All of the above templates are convolved with the filter response curves to generate model magnitudes. These response curves consist of u, g, r, i, z filter transmission functions for the observations taken by the Canada-France Hawaii Telescope (CFHT).

3   CLASSIFICATION COMBINATION METHODS

Building on the work in the field of ensemble learning, we combine the predictions from individual star-galaxy classification techniques using ensemble learning techniques known as Bayesian Model Combination (BMC) and a variant of an ensemble learning technique known as stacking. The main idea behind ensemble learning is to weigh the predictions from individual models and combine them to obtain a prediction that outperforms every one of them individually (**?**).

3.1   Unsupervised Binning

Given the variety of star-galaxy classification methods we are using, we fully expect the relative performance of the individual techniques to vary across the parameter space spanned by the data. For example, it is reasonable to expect supervised techniques to outperform other techniques in areas of parameter space that are well-populated with training data. Similarly, we can expect unsupervised approaches such as `SOM` or template fitting approaches to generally perform better when training data is either sparse or unavailable.

We therefore adopt the binning strategy similar to **?**. In this binning strategy, we allow different classifier combinations in different parts of parameter space by creating two-dimensional SOM representations of the full nine-dimensional magnitude-color space: $u, g, r, i, z, u-g, g-r, r-i$, and $i-z$. A SOM representation can be rectangular, hexagonal,

or spherical; here we choose a 10×10 rectangular topology to facilitate visualization as shown in Figure. 2. For all combination methods, we use only the OOB (cross validation) data contained in each cell to compute the relative weights for the base classifiers. The weights within individual cells are then applied to the test data to make the prediction.

Furthermore, we construct a collection of SOM representations and subsequently combine the predictions from each map into a meta-prediction. Given a training sample of N sources, we generate N_R random realizations of training data by perturbing the attributes with the measured uncertainty for each attribute. The uncertainties are assumed to be normally distributed. In this manner, we reduce the bias towards the data and introduce randomness in a systematic manner. For each random realization of a training sample, we create N_M bootstrap samples of size N to generate N_M different maps.

After all maps are built, we have a total of $N_R \times N_M$ probabilistic outputs for each of the N sources. To produce a single probability estimate for each source, one can take the mean, the median, or some other simple statistic. With a sufficient number of maps, we find that there is usually negligible difference between taking the mean and taking the median, and so we use the median in the following sections. We note that it is also possible to establish confidence intervals using the distribution of the probability estimates.

3.2   Weighted Average

The simplest approach to combine different combination techniques is to simply add the individual classifications from the base classifiers and renormalize the sum. In this case, the final probability is given by

$$P\left(S|\mathbf{x}, \mathbf{M}\right) = \sum_i P\left(S|\mathbf{x}, M_i\right), \tag{6}$$

where $\mathbf{M}$ is the set of models (`TPC`, `SOMc`, `HB`, and morphological separation in our work). We improve on this simple approach by using the binning strategy to calculate the weighted average of each bin separately, rather than globally.

3.3   Bucket of Models (BoM)

After the multi-dimensional input data have been binned, we can use the cross-validation data to choose the best model within each bin, and we use only that model within that specific bin to make predictions for the test data. We use the mean squared error (MSE; also known as Brier score (**?**)) as a classification error metric. We define MSE as

$$\mathrm{MSE} = \frac{1}{N} \sum_{i=0}^{N-1} \left(y_i - \hat{y}_i\right)^2, \tag{7}$$

where $\hat{y}_i$ is the actual truth value (e.g., 0 or 1) of the ith data, and y_i is the probability prediction made by the models. Thus, a model with the minimum MSE is chosen in each bin and is assigned a weight of one, and zero for all other models. However, the chosen model is allowed to vary between different bins.

3.4   Stacking

Instead of selecting a single model that performs best within each bin, we can train a learning algorithm to combine the

output values of several other base classifiers in each bin. An ensemble learning method of using a meta-classifier to combine lower-level classifiers is known as *stacking* or *stacked generalization* (**?**). Although any arbitrary algorithm can theoretically be used as a meta-classifier, a logistic regression or a linear regression is often used in practice. In our work, we use a single-layer multi-response linear regression algorithm, which often shows the best performance (**??**).

3.5 Bayesian Model Combination

We also use a model combination technique (**?**) known as Bayesian Model Combination (BMC). BMC uses Bayesian principles to generate an ensemble combination of different classifiers (**?**). The posterior probability that a source is a star is given by

$$P\left(S|\mathbf{x},\mathbf{D},\mathbf{M},\mathbf{E}\right) = \sum_{e\in\mathbf{E}} P\left(S|\mathbf{x},\mathbf{M},e\right) P\left(e|\mathbf{D}\right), \qquad (8)$$

where $\mathbf{D}$ is the data set, and e is an element in the ensemble space $\mathbf{E}$ of possible model combinations. By Bayes' Theorem, the posterior probability of e given $\mathbf{D}$ is given by

$$P\left(e|\mathbf{D}\right) = \frac{P\left(e\right)}{P\left(\mathbf{D}\right)} \prod_{d\in\mathbf{D}} P\left(d|e\right) \propto P\left(e\right) \prod_{d\in\mathbf{D}} P\left(d|e\right). \qquad (9)$$

Here, the product of $P\left(d \mid e\right)$ is over all individual data d in the training data $\mathbf{D}$, and $P\left(\mathbf{D}\right)$ is merely a normalization factor and not important.

For binary classifiers whose output is either zero or one (e.g., a cut-based morphological separation), we assume that each example is corrupted with an average error rate ϵ. This means that $P\left(d|e\right) = 1 - \epsilon$ if the combination e correctly predicts class $\hat{y}_i$ for the ith object, and $P\left(d|e\right) = \epsilon$ if it predicts an incorrect class. The average rate ϵ can be estimated by the fraction $\left(M_g + M_s\right)/N$, where M_g is the number of true galaxies classified as stars, M_s is the number of true stars classified as galaxies, and N is the total number of sources. Equation 9 then becomes

$$P\left(e|\mathbf{D}\right) \propto P\left(e\right)\left(1 - \epsilon\right)^{N_s + N_g} \left(\epsilon\right)^{M_s + M_g}. \qquad (10)$$

For probabilistic classifiers, we can directly use the probabilistic predictions and write Equation 9 as

$$P\left(e|\mathbf{D}\right) \propto P\left(e\right) \prod_{i=0}^{N-1} \hat{y}_i y_i + \left(1 - \hat{y}_i\right)\left(1 - y_i\right). \qquad (11)$$

Although the space $\mathbf{E}$ of potential model combinations is in principle infinite, we can produce a reasonable finite set of potential model combinations by using sampling techniques. In our implementation, the weights of each combination of the base classifiers is obtained by sampling from a Dirichlet distribution. We first set all alpha values of a Dirichlet distribution. We then sample this distribution q times to obtain q sets of weights. For each combination, we assume a uniform prior and calculate $P\left(e|\mathbf{D}\right)$ using Equation 9. We select the combination with the highest $P\left(e|\mathbf{D}\right)$, and update the alpha values by adding the weights of the most probable combination to the current alpha values. The next q weight sets of weights are drawn using the updated alpha values.

We continue the sampling process until we reach a predefined number of combinations, and finally use Equation 8 to compute the posterior probability that a source is a star (or a galaxy). In this paper, we use a q value of three, and 1,000 model combinations were considered.

We also use a binned version of the BMC technique, where we use a SOM representation to apply different model combinations for different regions of the parameter space. We however note that introducing randomness though the construction of different SOM representations does not show significant improvement over using only one single SOM representation. This similarity is likely due to the randomness that has already been introduced by the sampling from the Dirichlet distribution. Thus, our BMC technique uses one SOM, while other base models (WA, BoM, and stacking) generate N_R random realizations of N_M maps.

4 DATA

We use photometric data from the Canada-France-Hawaii Telescope Lensing Survey (CFHTLenS[4]; **???**). This catalog consits of more than twenty five million objects with a limiting magnitude of $i_{\text{AB}} \approx 25.5$. It covers a total of 154 square degrees in the four fields of CFHT Legacy Survey (CFHTLS; **?**) observed in the five photometric bands: u, g, r, i, and z.

We have cross-matched reliable spectroscopic galaxies from the Deep Extragalactic Evolutionary Probe Phase 2 (DEEP2; **??**), the Sloan Digital Sky Survey Data Release 10 (**?**, SDSS-DR10), the VIsible imaging Multi-Object Spectrograph (VIMOS) Very Large Telescope (VLT) Deep Survey (VVDS; **??**), and the VIMOS Public Extragalactic Redshift Survey (VIPERS; **?**), In the end, we have 8,545 stars and 57,843 galaxies available for the training and testing processes.

Our goal here is not to obtain the best classifier performance; for this we would have fine tuned individual base classifiers and chosen sophisticated models best suited to the particular properties of the CFHTLenS data. For example, **?** suggest that all objects with $i > 23$ in the CFHTLenS dataset may be classified as galaxies without significant incompleteness in the galaxy sample. Although this approach works because the high Galactic latitude fields of the CFHTLS contain relatively few stars, it is very unlikely that such an approach will meet the science requirements for the quality of star-galaxy classification in lower latitude, star-crowded fields. Rather, our goal for the CFHTLenS dataset is to demonstrate the usefulness of combining different classifiers even when the base classifiers may be poor or trained on partial data.

5 RESULTS AND DISCUSSION

In this section, we present the classification performance of the four different combination techniques, as well as the individual star-galaxy classification techniques on the CFHTLenS test data.

5.1 Classification Metrics

Probabilistic classification models can be considered as functions that output a probability estimate of each source to be

---

[4] http://www.cfhtlens.org/

in one of the classes (e.g., a star or a galaxy). Although the probability estimate can be used as a weight in subsequent analyses to improve or enhance a particular measurement (**?**), it can also be converted into a class label by using a threshold (probability cut). The simplest way to choose the threshold is to set it to a fixed value, e.g., $p_{\mathrm{cut}} = 0.5$. This is, in fact, what is often done (e.g., **??**). However, choosing 0.5 as a threshold is not the best choice for an unbalanced data set, where galaxies outnumber stars. Furthermore, setting a fixed threshold ignores the operating condition (e.g., science requirements, stellar distribution, misclassification costs) where the model will be applied.

When we have no information about the operating condition when evaluating the performance of classifiers, there are effective tools such as the Receiver Operating Characteristic (ROC) curve (**?**). An ROC curve is a graphical plot that illustrates the true positive rate versus the false positive rate of a binary classifier as its classification threshold (probability cut) is varied. The Area Under the Curve (AUC) summarizes the curve information in a single number, and can be used as an assessment of the overall performance.

In astronomical applications, the operating condition usually translates to the completeness and purity requirements of the star/galaxy sample, We define the galaxy *completeness* c_g (also known as recall or sensitivity) as the fraction of the number of true galaxies classified as galaxies out of the total number of true galaxies,

$$c_g = \frac{N_g}{N_g + M_g}, \tag{12}$$

where N_g is the number of true galaxies classified as galaxies and M_g is the number of true galaxies classified as stars. We define the galaxy *purity* p_g (also known as precision or positive predictive value) as the fraction of the number of true galaxies classified as galaxies out of the total number of objects classified as galaxies,

$$p_g = \frac{N_g}{N_g + M_s}, \tag{13}$$

where M_s is the number of true stars classified as galaxies. Star completeness and purity are defined in a similar manner.

One of the advantages of a probabilistic classification is that the threshold can be adjusted to produce a more complete but less pure sample, or a less complete but more pure one. To compare the performance of probabilistic classification techniques with that of the morphological separation, which has a fixed completeness ($c_g = 0.9964$, $c_s = 0.7145$) at a certain purity ($p_g = 0.9484$, $p_s = 0.9666$), we adjust the threshold of probabilistic classifiers until the galaxy completeness matches that of the morphological classifier to compute p_g at $c_g = 0.9964$. Similarly, the star purity p_s at $c_s = 0.7145$ is computed by adjusting the threshold values until the star completeness of each classifier is equal to that of the morphological classifier.

We can also compare the performance of different classification techniques by assuming an arbitrary operating condition. For example, weak lensing science measurements of the DES require $c_g > 0.960$ and $p_g > 0.778$ to control both the statistical and systematic errors on the cosmological parameters, and $c_s > 0.250$ and $p_s > 0.970$ for stellar Point Spread Function (PSF) calibration (**?**). Although these values will likely be different for the science cases of the CFHTLenS data, we adopt these values to compare the classification performance at a reasonable operating condition. Thus, we compute p_g at

Table 1. The definition of the classification performance metrics.

Metric	Meaning
AUC	Area under the Receiver Operating Curve
MSE	Mean squared error
c_g	Galaxy completeness
p_g	Galaxy purity
c_s	Star completeness
p_s	Star purity
$p_g(c_g = x)$	Galaxy purity at x galaxy purity
$p_s(c_s = x)$	Star purity at x star purity

$c_g = 0.960$ and c_s at $p_s = 0.250$. We also use the MSE defined in Equation 7 as a classification error metric.

5.2   Classifier Combination

We present in Table 2 the classification performance obtained by applying the four different combination techniques, as well as the individual star-galaxy classification techniques, on the CFHTLenS test data. The bold entries highlight the best technique for any particular metric. The first four rows show the performance of four individual star-galaxy classification techniques. Given the wealth of training data, it is not surprising that our supervised machine learning tehcnique TPC outperforms other unsupervised technique. TPC is thus shown in the first row as the benchmark.

The simplest of the combination techniques, WA and BoM, generally do not perform better than TPC. It is also interesting that, even with binning the parameter space and selecting the best model within each bin, BoM almost always chooses TPC as the best model, and therefore gives the same performance as TPC in the end. However, our BMC and stacking techniques have a similar performance and often outperform TPC. Although TPC shows the best performance as measured by the AUC, BMC shows the best performance in all other metrics.

In Figure 2, we show the mean CFHTLenS i-band magnitude in the top left panel and the fraction of stars in each cell in the top right panel. The bottom two panels show the mean $u - g$ and $g - r$ colors. These two-dimensional maps clearly shows the ability of the SOM to preserve relationships between sources when it projects the full nine-dimensional space to the two-dimensional map. The SOM mapping is a non-linear representation of all magnitudes and colors, and thus these SOM maps should only be used to provide guidance.

We can also use the same SOM to determine the relative weights for the four individual classification methods for each cell. We present the four weight maps for the BMC technique in Figure 3. In these maps, a redder color indicates a higher weight, or equivalently that the corresponding weight performs better in that region. These weight maps demonstrate the variation in the performance of the individual techniques across the two-dimensional parameter space defined by the SOM. Not surprisingly, the morphological separation performs best in the top left corner of the i-band magnitude map, which corresponds to the brightest CFHTLenS magnitudes $i \lesssim 20$. On the other hand, TPC seems to perform best in the region that corresponds to intermediate magnitudes $20 \gtrsim i \lesssim 22.5$ and $1.5 < u - g < 3.0$. Our unsupervised learning method SOMc performs relatively better at fainter magnitudes $i > 21.5$ with $0 < u - g < 0.5$ and $0 < g - r < 0.5$. Although HB shows the worst performance when there exists ample training data, BMC still utilizes information from HB to produce an overall

Table 2. A summary of the classification performance metrics for the four individual methods and the four different classification combination methods as applied to the CFHTLenS data, with no cut applied to the training data set. The definition of the metrics is summarized in Table 1. The bold entries highlight the best performance values within each column.

Classifier	AUC	MSE	p_g ($c_g = 0.9964$)	p_s ($c_s = 0.7145$)	p_g ($c_g = 0.9600$)	p_s ($c_s = 0.2500$)
TPC	**0.9870**	0.0208	0.9714	0.9838	0.9918	0.9977
SOMc	0.9683	0.0452	0.9125	0.8454	0.9788	0.9551
HB	0.9403	0.0705	0.9219	0.7017	0.9471	0.6963
Morphology	-	0.0397	0.9597	0.9666	-	-
WA	0.9806	0.0266	0.9755	0.9926	0.9872	0.9977
BoM	0.9870	0.0208	0.9714	0.9838	0.9918	0.9977
Stacking	0.9842	0.0194	0.9752	0.9902	0.9918	1.0000
BMC	0.9852	**0.0174**	**0.9800**	**0.9959**	**0.9924**	1.0000
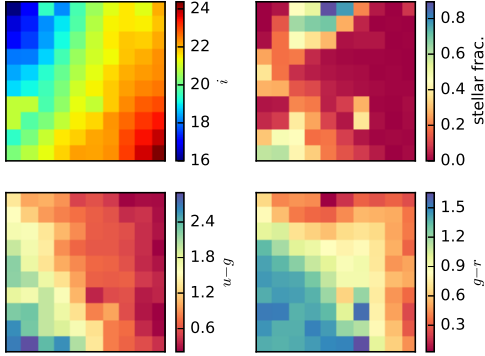
Figure 2. A two-dimensional 10×10 SOM representation showing the mean i-band magnitude (top left), the fraction of true stars in each cell (top right), and the mean values of $u - g$ and $g - r$ for the cross validation data.
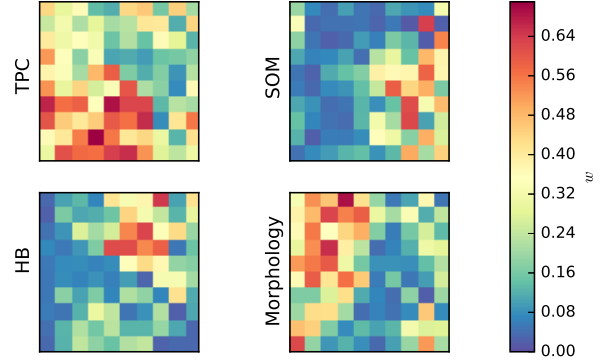
Figure 3. A two-dimensional 10×10 SOM representation showing the relative weights for the BMC combination technique applied to the four individual methods for the CFHTLenS data.

improvement in performance, especially at intermediate magnitudes $20 \gtrsim i \lesssim 22$.

In Figure 4, we compare the star and galaxy purity values for morphological separation, TPC, and BMC techniques as a function of i-band magnitude. Although morphological separation shows a slightly better performance at bright magnitudes $i < 21$, BMC outperforms both morphological separation and TPC at faint magnitudes $i > 21$. As shown in the histogram, the histogram peaks at $i \sim 22$, and BMC therefore outperforms the morphological separation technique for the majority of objects. It is also clear that BMC outperforms TPC over all magnitudes. BMC can accomplish this by combining information from all base classifiers, e.g., giving more weight to the morphological separation method at bright magnitudes.

5.3 The Quality of Training Data

It is very costly in terms of telescope time to obtain a large sample spectroscopic observations down to the limiting magnitude of a photometric sample. Thus, we investigate the impact of training set quality by imposing various magnitude and z cuts to decrease the size of the training set.

In Figure. 5, we present a visual comparison between different classification techniques when various magnitude cuts are applied.

In Figure. 6, we also present the result of imposing various z cuts.

5.4 Insufficient Training Data

We also investigate the impact of training set quality by analyzing in detail a more realistic case where the training data is available only for a small number of objects at bright magnitudes. To emulate this scenario, we only use objects that have spectroscopic labels from the VVDS 0226-04 field (which is located within the CFHTLS W1 field) and impose a magnitude cut of $i < 22.0$ in the training data, leaving us a training set with 1,365 objects.

We apply the same four star-galaxy classification techniques and four different combination methods, and test them on the same test data. We present in Table 3 the same six metrics for each method, and highlight the best method for each metric. Overall, the results obtained for the reduced data set are remarkable. With poor training data, our data-driven methods, TPC and SOMc, suffer a significant decrease in performance, although they still in general perform better than the template fitting algorithm HB. The performance of our morphological separation method does not depend on the training data, and shows the best result in the MSE metric. It also outperforms other base classifiers in galaxy purity at galaxy completeness of 0.9964 and in star purity at star completeness of 0.7145.

Without sufficient training data, the advantage of classification combination techniques is more obvious. Even WA, the simplest of combination techniques, outperforms all individual classification techniques. Interestingly, although TPC does not perform better than morphological separation, BoM
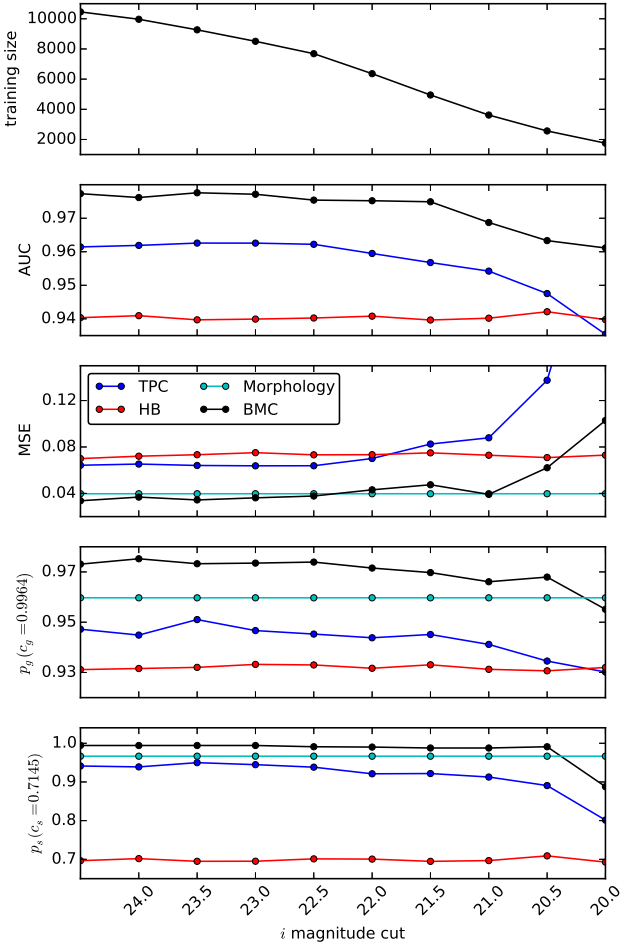
Figure 5. The classification performance metrics for TPC, HB, morphology, and BMC as applied to the CFHTLenS data in the VVDS field with various magnitude cuts. The top panel shows the number of sources in the training set at corresponding magnitude cuts. We show only one of the four combination methods, BMC, which has the best overall performance.
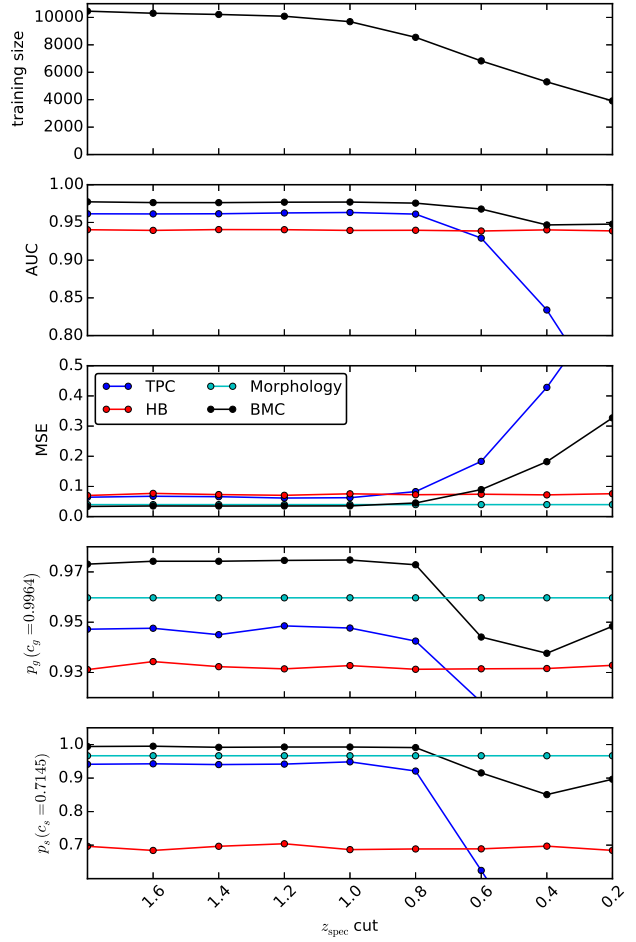
Figure 6. Same as Figure. 5 using $z_{\rm spec}$ cuts.

Table 3. A summary of the classification performance metrics for the four individual methods and the four different classification combination methods as applied to the CFHTLenS data in the VVDS field with a magnitude cut of $i < 22.0$. The definition of the metrics is summarized in Table 1. The bold entries highlight the best performance values within each column.

Classifier	AUC	MSE	$p_g\ (c_g = 0.9964)$	$p_s\ (c_s = 0.7145)$	$p_g\ (c_g = 0.9600)$	$p_s\ (c_s = 0.2500)$
TPC	0.9601	0.0728	0.9438	0.9329	0.9819	0.9950
SOMc	0.9008	0.1679	0.8843	0.5044	0.9244	0.7726
HB	0.8960	0.0894	0.9074	0.7516	0.9615	0.7793
Morphology	–	**0.0397**	0.9597	0.9666	–	–
WA	0.9639	0.0581	0.9613	0.9787	0.9756	1.0000
BoM	0.9601	0.0728	0.9438	0.9329	0.9819	0.9950
Stacking	0.9644	0.0613	0.9633	0.9835	0.9840	1.0000
BMC	**0.9738**	0.0437	**0.9676**	**0.9942**	**0.9878**	1.0000
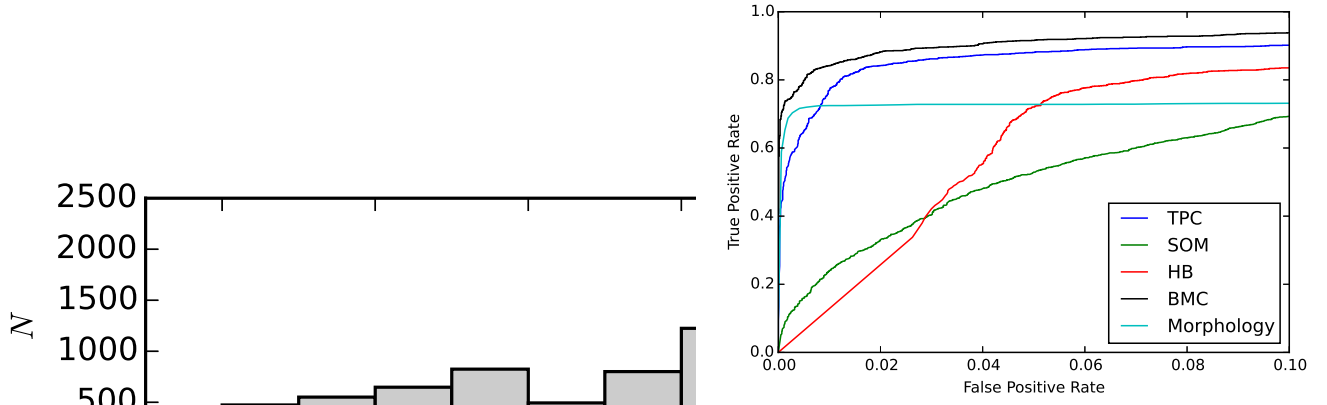
Figure 7. A magnified view of the ROC curve of four star-galaxy individual classification approaches (TPC, SOMc, HB, and morphology) and the best-performing combination technique (BMC), trained with the reduced data set. We show only one of the four combination methods, BMC, which has the best overall performance.
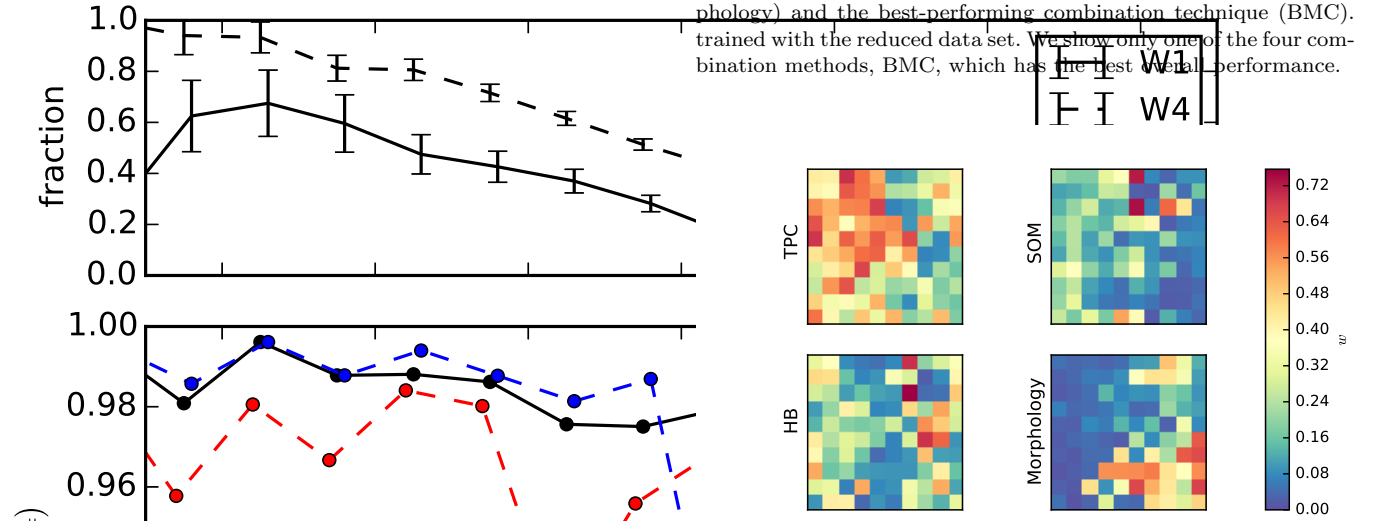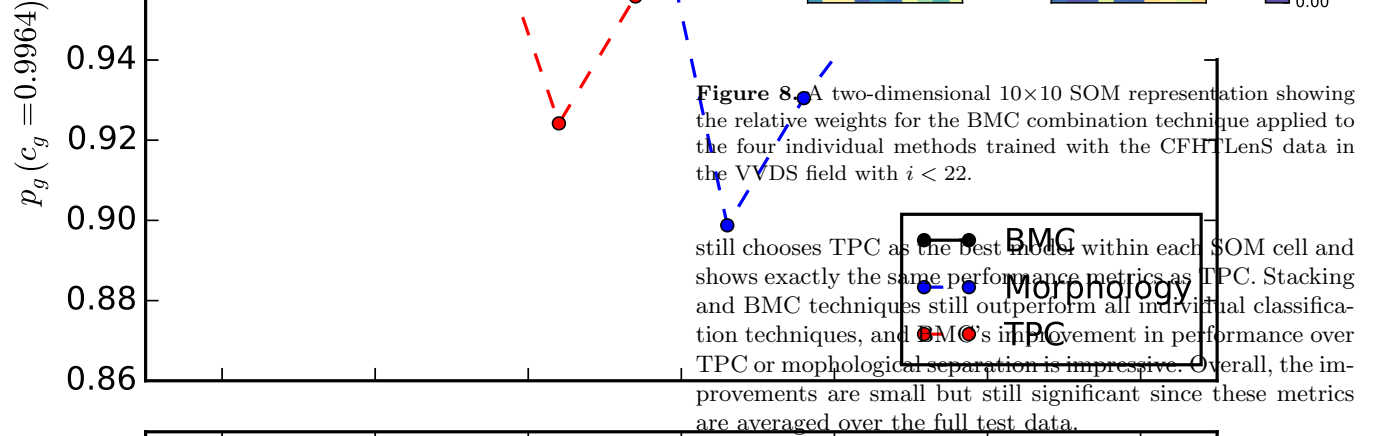

Figure 8. A two-dimensional 10×10 SOM representation showing the relative weights for the BMC combination technique applied to the four individual methods trained with the CFHTLenS data in the VVDS field with $i < 22$.

still chooses TPC as the best model within each SOM cell and shows exactly the same performance metrics as TPC. Stacking and BMC techniques still outperform all individual classification techniques, and BMC's improvement in performance over TPC or mophological separation is impressive. Overall, the improvements are small but still significant since these metrics are averaged over the full test data.
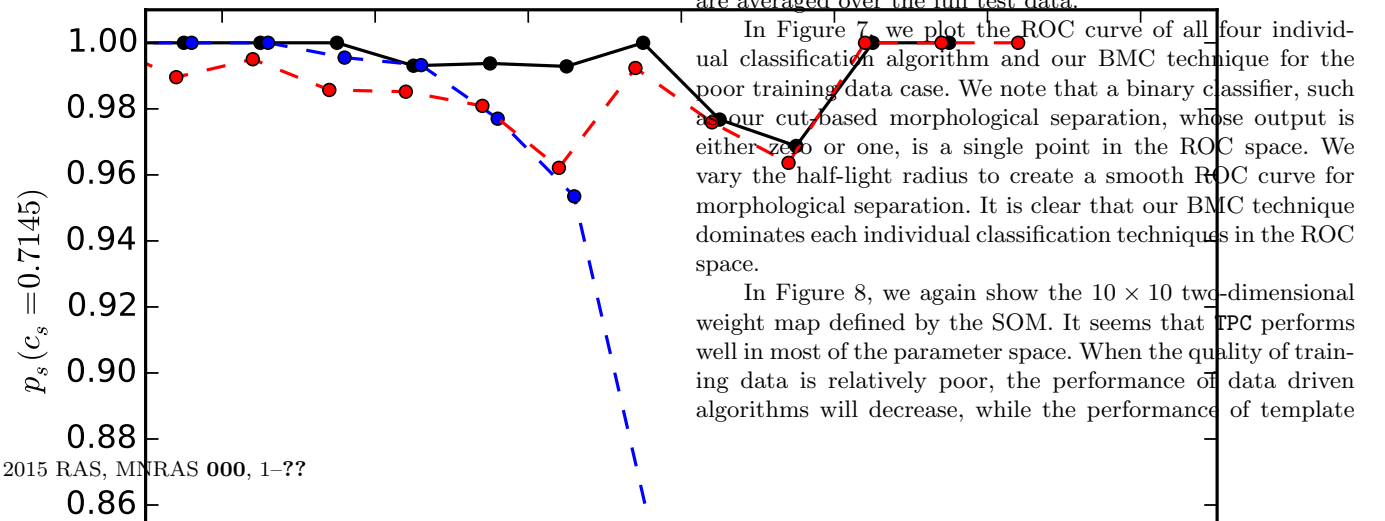
In Figure 7, we plot the ROC curve of all four individual classification algorithm and our BMC technique for the poor training data case. We note that a binary classifier, such as our cut-based morphological separation, whose output is either zero or one, is a single point in the ROC space. We vary the half-light radius to create a smooth ROC curve for morphological separation. It is clear that our BMC technique dominates each individual classification techniques in the ROC space.

In Figure 8, we again show the 10×10 two-dimensional weight map defined by the SOM. It seems that TPC performs well in most of the parameter space. When the quality of training data is relatively poor, the performance of data driven algorithms will decrease, while the performance of template

fitting algorithms such as HB is independent of training data. Thus, it is perhaps not surprising that BMC algorithm now uses information from `HB`, whereas it assigned almost no weight to `HB` when we had a high-quality training data. Another interesting pattern is that `SOMc` and morphological separation seem complementary; `SOMc` is weighted most strongly at fainter magnitudes, while the morphological separation method is weighted most strongly at brighter magnitudes. It is not surprising that the morphological separation method performs best at bright magnitudes, and BMC uses almost no morphological information at faint magnitudes.

We present the star and galaxy purity values of Table 3 as a function of i-band magnitude in Figure 4. It is clear that BMC outperforms both morphological separation and TPC classification techniques over all magnitudes. The galaxy purity of BMC is significantly better than that of TPC at bright magnitudes, $i \lesssim 21.5$, while they are similar at faint magnitudes. The star purity of BMC shows improvement over that of TPC at faint magnitudes, while they are similar at bright magnitudes. As suggested by the weight maps in Figure 8, BMC can accomplish this by combining information from all base classifiers, e.g., giving more weight to the morphological separation method at bright magnitudes. We can also see in the bottom two panels that the performance of morphological separation suffers at intermediate magnitudes $21 \lesssim i \lesssim 23$, while BMC shows consistently better performance over all magnitude ranges.

We also show the star and galaxy purity values of Table 3 as a function of photometric redshift in Figure **??**. Photo-z is estimated with the `BPZ` algorithm (**?**) and provided with the CFHTLenS photometric redshift catalogue (**?**). It is again clear that BMC outperforms both individual classification techniques over all redshift range.

We show the distribution of posterior star probabilities in Figures **??** and **??**. The histogram of spectroscopic galaxies is in blue, and the histogram of true stars is in red. It is interesting that the BMC technique assigns a probability $P(S)$ greater than 0.6 to almost no true galaxies in Figure **??**, presumably because BMC utilizes information from different types of classification techniques. This pattern is more pronounced in Figure **??**, where the $P(S)$ distribution of BMC for true galaxies falls off sharply at $P(S) \approx 0.95$, while morphological separation and TPC techniques classify some true galaxies as stars with absolute certainty.

To identify the regions in color-color space where our BMC technique struggles to classify stars and galaxies, we present the distribution over the color-color space for sources with $0.45 < P(S) < 0.55$ in Figure **??**. Not surprisingly, these regions correspond to where there is a significant overlap between stars and galaxies in the color space. It may be possible to improve the performance of star-galaxy classification by obtaining more information through spectroscopic follow-up, manual study, or citizen science projects, or by developing a classification technique specifically designed for these regions of the color space and combining it with other techniques in a Bayesian framework.

6   CONCLUSIONS

begin new text

We have presented and analyzed a novel star-galaxy classification framework for combining classifications from the CFHTLenS project. In particular, we use four independent star-galaxy classification techniques: a morphological separation method; `TPC`, a supervised machine learning technique based on prediction trees and a random forest; `SOMc`, an unsupervised machine leraning approach based on self-organizing maps and a random atlas; and `HB`, a hierarichical bayesian template-fitting method that we have modified and paralllized. Both `TPC` and `SOMc` are currently availble within a software package named `MLZ`[5]. Our implementaion of `HB` and `BMC`, as well as IPython notebooks that were used to produce the results in this paper, are available at `https://github.com/EdwardJKim/astroclass`.

end new text

When there's wealth of training data, TPC is so good that combination techniques show no significant improvement over TPC.

Even with poor (but reasonable) training data, TPC outperforms unsupervised methods.

In a more realistic case where the training data is poor, BMC should be used.

Probabilistic classification is better. Binary classification can be transformed into a probabilistic classification when combined with other models in a Bayesian framework.

We note that **?** analyzed different techniques for combining photometric redshift probability density functions (photo-z PDFs), and also found that BMC is in general the best photo-z PDF combination technique.

more here

REFERENCES

Ahn C. P. et al., 2014, ApJS, 211, 17
Ball N. M., Brunner R. J., Myers A. D., Tcheng D., 2006, ApJ, 650, 497
Benítez N., 2000, ApJ, 536, 571
Bertin E., Arnouts S., 1996, A&AS, 117, 393
Bohlin R. C., Colina L., Finley D. S., 1995, AJ, 110, 1316
Breiman L., 1996, Machine learning, 24, 49
Breiman L., 2001, Machine learning, 45, 5
Breiman L., Friedman J., Stone C. J., Olshen R. A., 1984, Classification and regression trees. CRC press
Brier G. W., 1950, Monthly weather review, 78, 1
Carrasco Kind M., Brunner R. J., 2013, MNRAS, 432, 1483
Carrasco Kind M., Brunner R. J., 2014a, MNRAS, 442, 3380
Carrasco Kind M., Brunner R. J., 2014b, MNRAS, 438, 3409
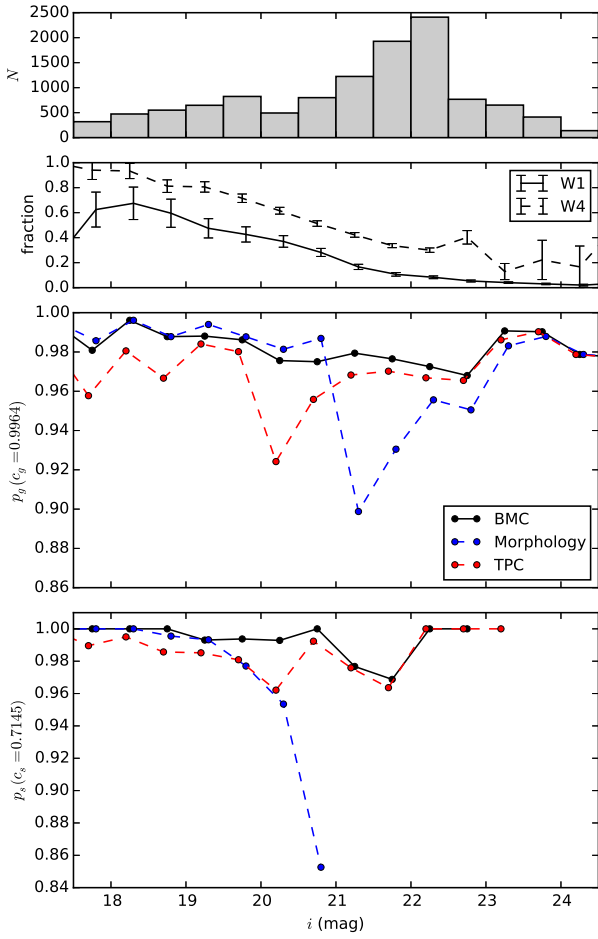Chabrier G., Baraffe I., Allard F., Hauschildt P., 2000, ApJ, 542, 464

[5] http://lcdm.astro.illinois.edu/code/mlz.html

Figure 9. Purity of morphological separation, TPC, and BMC techniques in Table 3 as a function of the i-band magnitude. The top panel shows the fraction of stars as a function of magnitude. the galaxy and star purity for TPC and BMC techniques. The bottom two panels show the galaxy and star purity for morphological separation and BMC technique. We use the same threshold values from Figure 4 in the bottom four panels
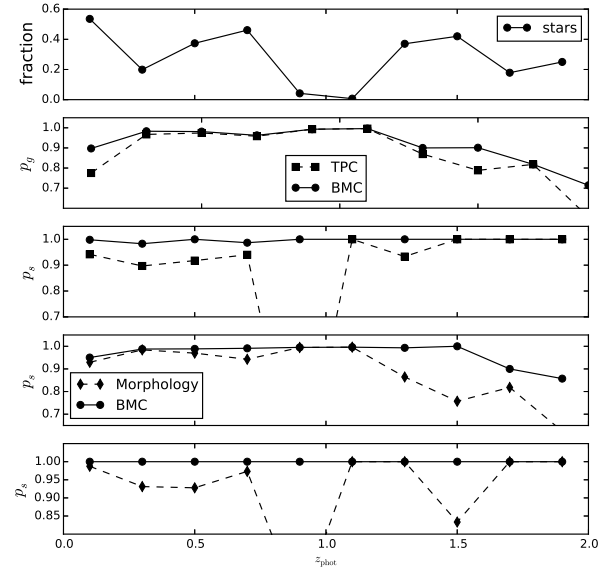
.

Figure 10. The same figures as Figure 4, but as a function of photometric redshift estimate (photo-z).

Coleman G. D., Wu C.-C., Weedman D. W., 1980, ApJS, 43, 393

Davis M. et al., 2003, in Society of Photo-Optical Instrumentation Engineers (SPIE) Conference Series, Vol. 4834, Discoveries and Research Prospects from 6- to 10-Meter-Class Telescopes II, Guhathakurta P., ed., pp. 161–172

Erben T. et al., 2013, MNRAS, 433, 2545

Fadely R., Hogg D. W., Willman B., 2012, ApJ, 760, 15

Foreman-Mackey D., Hogg D. W., Lang D., Goodman J., 2013, PASP, 125, 306

Garilli B. et al., 2014, A&A, 562, A23

Garilli B. et al., 2008, A&A, 486, 683

Górski K. M., Hivon E., Banday A. J., Wandelt B. D., Hansen F. K., Reinecke M., Bartelmann M., 2005, ApJ, 622, 759

Gwyn S. D., 2012, The Astronomical Journal, 143, 38

Henrion M., Mortlock D. J., Hand D. J., Gandy A., 2011, MNRAS, 412, 2286

Heymans C. et al., 2012, MNRAS, 427, 146

Hildebrandt H. et al., 2012, MNRAS, 421, 2355

Kaiser N., Squires G., Broadhurst T., 1995, ApJ, 449, 460

Kinney A. L., Calzetti D., Bohlin R. C., McQuade K., Storchi-Bergmann T., Schmitt H. R., 1996, ApJ, 467, 38

Kohonen T., 1990, Proceedings of the IEEE, 78, 1464

Kohonen T., 2001, Self-organizing maps, Vol. 30. Springer Science & Business Media

Kron R. G., 1980, ApJS, 43, 305

Le Fèvre O. et al., 2005, A&A, 439, 845

Messier C., 1781, Connoissance des Temps for 1784, 227

Monteith K., Carroll J. L., Seppi K., Martinez T., 2011, in Neural Networks (IJCNN), The 2011 International Joint
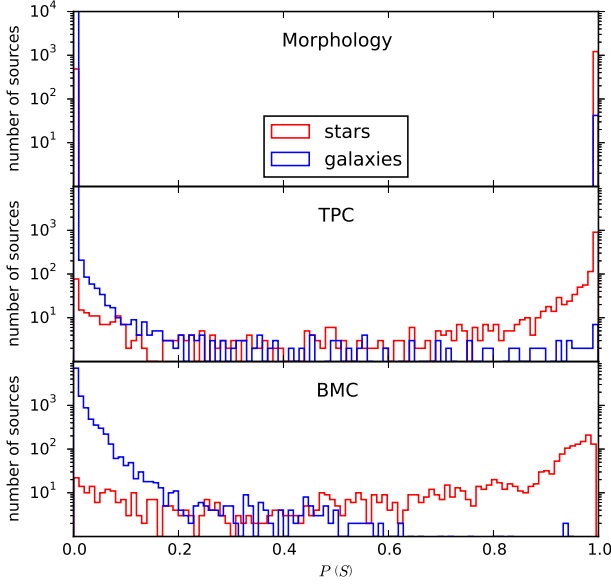
Figure 11. Histogram of the posterior probability that a source is a star for morphological separation (top), TPC (middle), and BMC (bottom) techniques for the entire training data (the CFHTLenS data in the DEEP2, SDSS, VIPERS, and VVDS fields as discussed in Section 5.2).
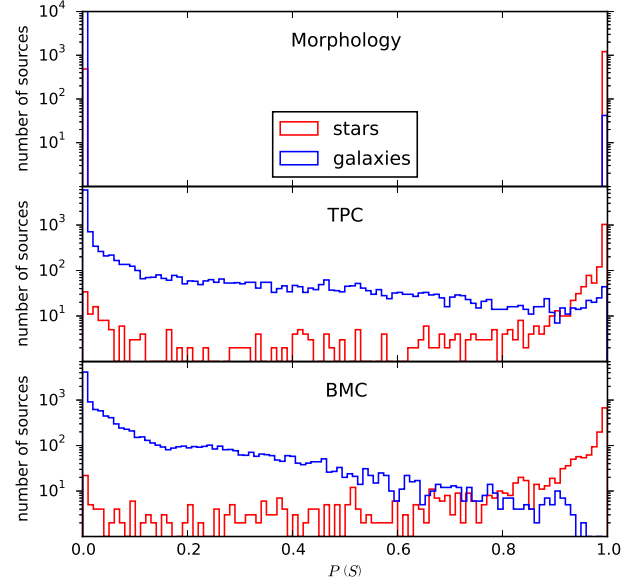
Figure 12. The same figures as Figure **??**, but for TPC and BMC trained with poor training data (the CFHTLenS data in the VDDS field with a magnitude cut of $i < 22$).
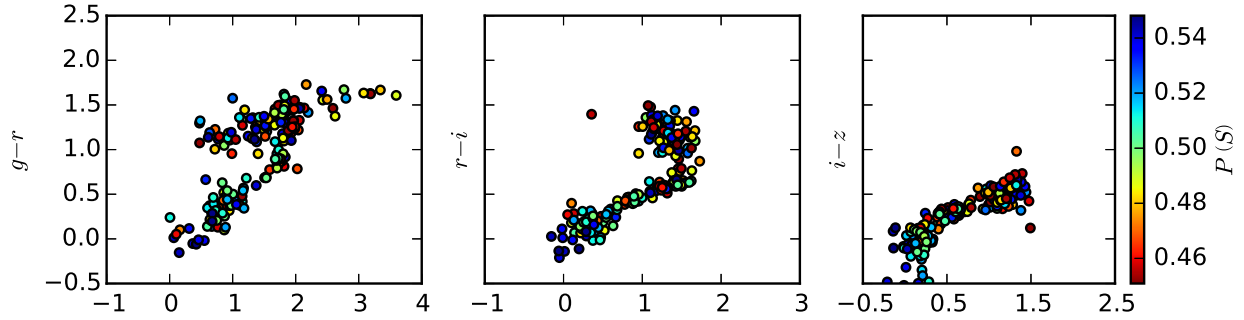

Figure 13. Color-color diagrams of sources with $0.45 < P(S) < 0.55$ when the BMC technique is applied to the poor training data.

Conference on, IEEE, pp. 2657–2663

Newman J. A. et al., 2013, ApJS, 208, 5

Odewahn S. C., Stockwell E. B., Pennington R. L., Humphreys R. M., Zumach W. A., 1992, AJ, 103, 318

Pickles A. J., 1998, PASP, 110, 863

Robin A. C. et al., 2007, ApJS, 172, 545

Rokach L., 2010, Artificial Intelligence Review, 33, 1

Ross A. J. et al., 2011, MNRAS, 417, 1350

Sebok W. L., 1979, AJ, 84, 1526

Soumagnac M. T. et al., 2013, ArXiv e-prints

Suchkov A. A., Hanisch R. J., Margon B., 2005, AJ, 130, 2439

Swets J. A., Dawes R. M., Monahan J., 2000, Scientific American, 83

Ting K. M., Witten I. H., 1999, J. Artif. Intell. Res.(JAIR), 10, 271

Valdes F., 1982, in Society of Photo-Optical Instrumentation Engineers (SPIE) Conference Series, Vol. 331, Instrumenta-

tion in Astronomy IV, pp. 465–472

Vasconcellos E. C., de Carvalho R. R., Gal R. R., LaBarbera F. L., Capelato H. V., Frago Campos Velho H., Trevisan M., Ruiz R. S. R., 2011, AJ, 141, 189

Weir N., Fayyad U. M., Djorgovski S., 1995, AJ, 109, 2401

Wolpert D. H., 1992, Neural networks, 5, 241

Yee H. K. C., 1991, PASP, 103, 396

This paper has been typeset from a TEX/ LATEX file prepared by the author.